

An endochronic model of material function and its application to plastic behavior of metals under asymmetric cyclic loadings

Wei-Ching Yeh[†]

Department of Mechanical Engineering, National Central University, Chung-Li, 32054, Taiwan, R.O.C.

Hsi-Yen Lin[‡]

Patent Division III, Intellectual Property Office, Ministry of Economic Affairs, R.O.C.

Jhen-Bo Jhao^{‡†}

Department of Mechanical Engineering, National Central University, Chung-Li, 32054, Taiwan, R.O.C.

(Received August 22, 2005, Accepted September 7, 2006)

Abstract. By using the incremental form of the endochronic theory of plasticity, a model of material function is proposed in this paper to investigate plastic behavior. By comparing the stress-strain hysteresis loop, the theory is shown to agree well with the experimental results, especially in the evolution of peak stress values of SAE 4340 steel loaded by cyclic loading with various amplitudes. Depending on the choice of material parameters, the present model can substantially result in six categories of material function, each of which can behave differently with respect to an identical deformation history. In addition, the present model of material function is shown to be capable of describing the behavior of erasure of memory of materials, as experimentally observed by Lamba and Sidebottom (1978).

Keywords: endochronic theory; cyclic loading conditions; material function; erasure of memory.

1. Introduction

A large number of models have been presented to describe the behavior of cyclic plasticity for different problems in literatures. The principal phenomena of cyclic plasticity, such as the Baushinger effect, cyclic hardening/softening, strain memory effect, ratcheting effect and out-of-phase hardening (additional hardening), have been extensively investigated by Lamba and Sidebottom (1978), Krempl and Lu (1984), Tanaka *et al.* (1985a,b), Chang and Lee (1986), Hopperstad (1995a,b), Calloch (1997), Kwofie (2003), Samson *et al.* (2004) and many others. The methods they used for

[†] Professor, Corresponding author, E-mail: wcyeh@cc.ncu.edu.tw

[‡] Ph.D., Executed Officer, E-mail: lce20262@tipo.gov.tw

^{‡†} Graduate Student

investigation of cyclic plasticity problems can be categorized according to different approaches. One of the methods is based on the macroscopic phenomenological approach, assuming that the polycrystalline material is homogeneous at the macro-level, and that yield surfaces depend on the stress, and strain measures as well as their rates. The other is based on the microscopic physical approach, involving the knowledge about microstructure of materials as suggested, e.g., by Dafalias and Aifantis (1990), Beaudoin *et al.* (1991), Ning and Aifantis (1996), Miehe *et al.* (1999), and Diard *et al.* (2004). Physical models based on micromechanics are advantageous to give an insight into the plastic behavior of materials, but the complexity of microstructure and deformation mechanisms in real materials, causing the complex expressions of the physical models and therefore spending more time to calculate, reduces their usefulness. Accordingly, although the phenomenological model, which usually defines a yield surface and a flow rule, seldom gives direct insight into the physical reason of the observed phenomena, yet it is an important topic in association with the development of more realistic constitutive equations in plasticity for the simulation of elasto-plastic problems. Moreover, in developing the phenomenological model, cyclic plasticity effects may be described by employing in the constitutive equation with a set of internal variables and some material parameters, which should be calibrated by using an experimental data. Specifically, the state of the material is either described by the present values of observable variables and a set of internal state variables as in multisurface theory by Mroz (1967), and two-surface theory by Krieg (1975) and by Dafalias and Popov (1976), or described by the present values and the past history of observable variables as in endochronic theory by Valanis (1971, 1980).

The purpose of this article is to propose an endochronic model of material function capable of describing cyclic plastic behavior of metals. In association with the endochronic theory of plasticity, the present model is applied to SAE 4340 steel uniaxially loaded by cyclic loading of various amplitudes, and is demonstrated to be capable of describing the behavior of erasure of memory of metals in the axial-torsional space. The behavior of erasure of memory was experimentally found by Lamba and Sidebottom (1978). However, the theory, initially proposed by Valanis (1971), is developed using the concept of irreversible thermodynamics of internal states variables. It considers the current state of stress as a function of entire history of deformation, and furthermore introduces the notion of intrinsic time ζ which may be regarded as a material property accumulating the loading histories of the material. Initially, the intrinsic time was defined by the norm of total strain tensor to account for the history of deformation, but it may cause discrepancy in the condition of cyclic loading path, resulting in hysteresis loop of stress-strain which could never closure. Such a discrepancy was much criticized by Sandler (1978) and Rivlin (1981). For this reason, Valanis (1980) redefined the intrinsic time by the norm of plastic strain tensor as follows:

$$d\zeta^2 = d\theta_{ij} \cdot K_{ijkl} \cdot d\theta_{kl} \quad (1)$$

where ζ represents the intrinsic time, $d\theta_{ij}$ represents a liked incremental plastic strain tensor defined by:

$$d\theta_{ij} = de_{ij} - \kappa_1 \frac{ds_{ij}}{2\mu_0} \quad (2)$$

In Eqs. (1) and (2), K_{ijkl} is a positive definite material tensor of fourth order related to $d\theta_{ij}$; ds_{ij} represents the incremental deviatoric stress tensor; μ_0 represents the shear modulus; κ_1 is a parameter ranging between 0 and 1. We note that Eq. (2) is expressed as plastic incremental strain tensor ($d\theta_{ij} = de_{ij}^p$) when $\kappa_1 = 1$.

A material function $f(z)$ is also introduced in the theory to fulfill the description of the hardening or softening behaviors of materials, and may be defined as follows:

$$f(z) = \frac{d\zeta}{dz} \quad (3)$$

where z is called intrinsic time scale. According to Eq. (1), the intrinsic time ζ having the same value is determined for different materials experiencing identical loading history. However, due to presence of the material function $f(z)$ as given by Eq. (3), it is clear that corresponding to the same value of ζ , the intrinsic time scale z can be determined distinctively when the employed $f(z)$ is dissimilar. Since the intrinsic time scale z can be physically interpreted as an internal clock accounting for the loading effect exerted upon materials, (e.g., Valanis 1980, 1984, Wu and Yip 1981, Watanabe and Atluri 1986, Yeh *et al.* 1994, Pan *et al.* 1997, 1999) the material function $f(z)$ physically characterizes the plastic behaviors of materials. For hardening materials, the strength is increasing in proportion to the loading accumulation, therefore the corresponding material function $f(z)$ must be monotonically increasing along with the accumulation of the intrinsic time scale z . On the contrary, $f(z)$ must be a monotonic decreasing function for softening materials. Moreover, in order to comply with the experimental observation (e.g., Krempl and Lu 1984, Tanaka *et al.* 1985a,b) that the stress-strain hysteresis loop of stress-strain would finally tend to a steady state as the loading strain is accumulated to an adequate level, a saturated value of the material function $f(z)$ is finally demanded to fulfill the phenomenon.

Valanis (1971) proposed a model of material function, expressed as follows:

$$f(\zeta) = 1 + \beta\zeta \quad (4)$$

where β is a constant. However, the model of Eq. (4) could never predict well the steady state phenomenon of material under any specific loading condition as a result of the value of $f(\zeta)$ proportionally increasing along with the intrinsic time. In order to eliminate the deficiency of the above model and also to attain a more reasonable simulation of the plastic behaviors of materials, Wu and Yip (1981) further proposed an exponential form of material function,

$$f(z) = c - (c - 1) \cdot e^{-\beta z} \quad (5)$$

where c and β are both constants. According to Eq. (5), since the evolution of the function $f(z)$ is initially from 1 to c at its steady state as a loading condition proceeds, the constant $c > 1$ which characterizes a monotonic increasing $f(z)$ corresponds to the material behaving strain hardening, and the constant $c < 1$ which characterizes a monotonic decreasing $f(z)$ corresponds to that behaving strain softening. The rate of change of $f(z)$, however, is determined by β value dominating saturation rate of material.

Wu *et al.* (1986) have successfully applied the material function defined by Eq. (5) to verify 304 stainless steel under in-phase and out-of-phase plastic-strain paths. However, the results of experiment (e.g., Cailletaud 1984, Chang and Lee 1986, Ellyin and Wolodko 1997, Basuroychowdhury and Voyiadjis 1998) show that a material, in general, would behave considerably uneven hardening effects under these two different types of strain paths. It seems reasonable that the material function $f(z)$ given by Eq. (5) is considered in terms of qualitative comparison rather than quantitative analysis, and therefore cannot appropriately describe the Bauschinger effect, one of the results of

strain anisotropy occurring in cyclic loading condition. For this reason, Yeh (1995) modified Eq. (5) and proposed a material function as follows:

$$f(z) = c - (c - 1) \cdot e^{-\beta(z - z_{ref})} \quad (6)$$

where z_{ref} is called the reference intrinsic time corresponding to a plastic state at which the loading direction changes. Note that the initial value of z_{ref} is set zero.

According to Eq. (6), the material function $f(z)$ will be reset to 1, whenever loading direction changes, and then gradually increase or decrease to saturation value c . In particular, for a monotonic loading condition (loading direction keeps unchanged), since the reference intrinsic time z_{ref} is always equal to zero, Eq. (5) can be recovered from Eq. (6) obviously. The material function given by Eq. (6) was successfully applied by Yeh (1995) and Yeh *et al.* (1996) to predict the plastic behavior of 304 stainless steel under biaxial loading condition. In the work of Yeh (1995), a conclusion was made that the result determined from Eq. (6) is more accurate than that from Eq. (5) in predicting the Bauschinger effect by comparing with the experimental result. In the work of Yeh *et al.* (1996), the application of Eq. (6) demonstrated that the evolution of yield surfaces of 304 stainless under in-phase cyclic loading condition is simulated in a good agreement with the experimental findings. Even so, due to the fact that the saturation value c appearing in Eqs. (5) and (6) is a constant, it is difficult for the theory to describe well the experimental results of Shiao (2000), that the peak stress values would keep changing irregularly as a specified cyclic loading condition proceeded. Accordingly, in this article we are motivated to propose a model of the material function being capable of describing the plastic behavior of the material subjected to specific cyclic loading condition as was employed in Shiao (2000). The constitutive equation associated with the present model is due to Murakame and Read (1989) who derived an incremental form of the endochronic theory of plasticity.

In order to verify the validity and capability of the present model, the experimental results obtained by Shiao (2000), and Lamba and Sidebottom (1978) were employed. The experimental results of Shiao (2000), which were compared with theoretical predictions for discussion, were obtained from the circular rod specimens of SAE4340 alloy steel subjected to uniaxially cyclic loading with various amplitudes. The experiment of Lamba and Sidebottom (1978) includes a series of biaxial loading tests for thin walled copper OFHC (oxygen free high conductivity), from which the so-called ‘erasure of memory’ was defined theoretically. More specifically, erasure of memory may be stated as follows. If subsequent strain paths, after the material had been cyclically stabilized under 90 deg out-of-phase cycling, remain in the region enclosed by the former, one “big” cycle always brings the material back to one particular stable plastic state, corresponding to that “big” cycle, even though many smaller cycles intervene. For studying a better insight into the behavior of materials in cyclic loading, in this study the implementation of the present model were also employed for simulating the effect of erasure of memory, experimentally found by Lamba and Sidebottom (1978).

2. The incremental form of endochronic theory of plasticity

2.1 Constitution equation of endochronic theory of plasticity

Assuming that materials being considered are isotropic and plastically incompressible, the

constitutive equation proposed by Valanis (1971) for small deformation can be expressed as follows:

$$s_{ij} = 2 \int_0^z \rho_{ijkl}(z-z') \frac{\partial \theta_{kl}}{\partial z'} dz' \tag{7}$$

$$\rho_{ijkl} \approx \begin{pmatrix} U & 0 & 0 & 0 & 0 & 0 \\ 0 & U & 0 & 0 & 0 & 0 \\ 0 & 0 & U & 0 & 0 & 0 \\ 0 & 0 & 0 & V & 0 & 0 \\ 0 & 0 & 0 & 0 & V & 0 \\ 0 & 0 & 0 & 0 & 0 & V \end{pmatrix}$$

$$U(z) = \frac{1}{1-\kappa_1} e^{-\left(\frac{a_0}{1-\kappa_1}\right)z} + \sum_{i=1}^{n-1} A_i e^{-a_i z} + A_0$$

$$V(z) = \frac{1}{1-\kappa_1} e^{-\left(\frac{b_0}{1-\kappa_1}\right)z} + \sum_{i=1}^{n-1} B_i e^{-b_i z} + B_0$$

$$d\theta_{ij} = de_{ij} - \kappa_1 \frac{ds_{ij}}{2\mu_0}$$

In the above equation, s_{ij} and e_{ij} are the deviatoric stress and strain, respectively; μ_0 is the shear modulus, and κ_1 a parameter ranging between 0 and 1; ρ_{ijkl} is called kernel function consisting of $U(z)$ and $V(z)$, where a_i, A_i, b_i and $B_i (i = 0, 1, \dots, n-1)$ are all material constants. In the case of $U(z) = V(z)$, Eq. (7) is an isotropic form. Otherwise, it is anisotropic and therefore leads to different behaviors in shear and normal directions, respectively.

Due to $U(z)$ and $V(z)$ of the kernel function in Eq. (7) having weak singularity feature at $z = 0$, the kernel function is required not only to be infinite, but also to have a monotonic decaying feature. Such a kernel function, proposed by Valanis and Fan (1983), may be expressed in terms of a set of finite exponential decaying functions:

$$U(z) \cong \sum_{r=1}^n C_r e^{-\alpha_r z}$$

$$V(z) \cong \sum_{r=1}^n C_r^* e^{-\alpha_r^* z} \tag{8}$$

where C_r, C_r^*, α_r and α_r^* are material constants.

By using the Leibnitz's differential rule, Murakami and Read (1989) transformed Eq. (7) into an incremental form of the constitutive equation of endochronic theory of plasticity. The relationship between the total stress increment $d\sigma_{ij}$ and total strain increment $d\varepsilon_{ij}$ can be expressed as:

$$d\sigma_{ij} = p_1 d\varepsilon_{ij} + p_2 d\varepsilon_{kk} \delta_{ij} + p_3 \sum_{r=1}^n \alpha_r (\sigma_{ij} - \sigma_m \delta_{ij})_r dz, \quad i = j$$

$$d\sigma_{ij} = p_1^* d\varepsilon_{ij} + p_2^* d\varepsilon_{kk} \delta_{ij} + p_3^* \sum_{r=1}^n \alpha_r^* (\sigma_{ij} - \sigma_m \delta_{ij})_r dz, \quad i \neq j \quad (9)$$

where the summation terms on r can further be expanded step by step as follows:

$$\begin{aligned} (\sigma_{ij} - \sigma_m \delta_{ij})_r^{(k)} &= (s_{ij})_r^{(k)} \equiv (s_{ij})_r^{(k-1)} + (ds_{ij})_r^{(k-1)}, \quad k \geq 1 \\ &= \left[(s_{ij})_r + \frac{2C_r}{1 + \frac{U(0)}{u_0}} (d\varepsilon_{ij} - d\varepsilon_m \delta_{ij}) - \frac{\alpha_r (s_{ij})_r}{1 + \frac{U(0)}{u_0}} dz \right]^{(k-1)}, \quad i = j \end{aligned}$$

or

$$= \left[(s_{ij})_r + \frac{2C_r^*}{1 + \frac{V(0)}{u_0}} (d\varepsilon_{ij} - d\varepsilon_m \delta_{ij}) - \frac{\alpha_r^* (s_{ij})_r}{1 + \frac{V(0)}{u_0}} dz \right]^{(k-1)}, \quad i \neq j$$

In the above equations, k denotes the computation of k_{th} step; σ_m and ε_m are the mean stress and mean strain, equal to $\sigma_{kk}/3$ and $\varepsilon_{kk}/3$ respectively, and δ_{ij} the Kronecker delta function; all the material constants can be expressed as

$$\begin{aligned} p_1 &= \frac{2U(0)}{1 + \frac{U(0)}{\mu_0}}, & p_2 &= K - \frac{2U(0)}{3\left(1 + \frac{U(0)}{\mu_0}\right)}, & p_3 &= \frac{-1}{1 + \frac{U(0)}{\mu_0}} \\ p_1^* &= \frac{2V(0)}{1 + \frac{V(0)}{\mu_0}}, & p_2^* &= K - \frac{2V(0)}{3\left(1 + \frac{V(0)}{\mu_0}\right)}, & p_3^* &= \frac{-1}{1 + \frac{V(0)}{\mu_0}} \end{aligned}$$

where K represents the bulk modulus of elasticity. We note that at the initial step $k=1$, the deviatoric stress $(s_{ij})_r^{(0)}$ equals to zero.

2.2 Proposed material function

In order to more precisely describe the cyclic plastic behavior of materials, an endochronic model of material function $f(z)$ is proposed as follows:

$$f(z) = c(z_{ref}) - [c(z_{ref}) - 1] \cdot e^{-\beta_1(z - z_{ref})} \quad (10)$$

where

$$c(z_{ref}) = d - \frac{d-1}{h} (1 - e^{-\beta_2 z_{ref}})$$

In the above equation, $c(z_{ref})$ is a function depending on loading path, and can be referred to as a saturation function of the material function $f(z)$ during each step of a cyclic loading path; β_1 is a material constant in relation to the rate of change of $f(z)$ characterizing steady state condition of

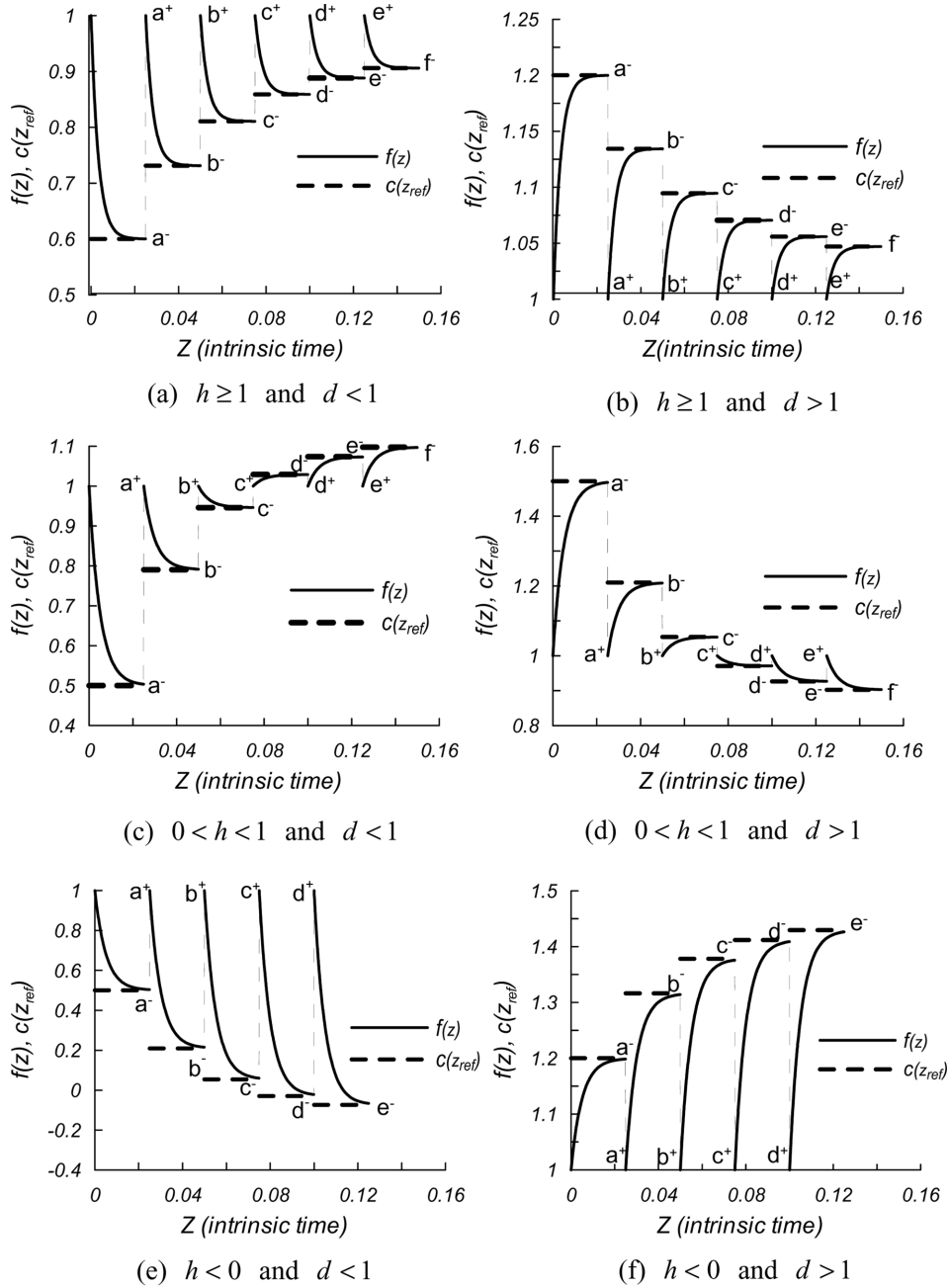


Fig. 1 Schematic representation of the functions $f(z)$ and $c(z_{ref})$

materials, and z_{ref} a reference intrinsic time as defined by Eq. (6); d , h and β_2 are also material constants, where the material constant β_2 dominates the rate of change of $c(z_{ref})$ value, and the other constants, d and h , which feature the property of the material function $f(z)$, will be discussed subsequently.

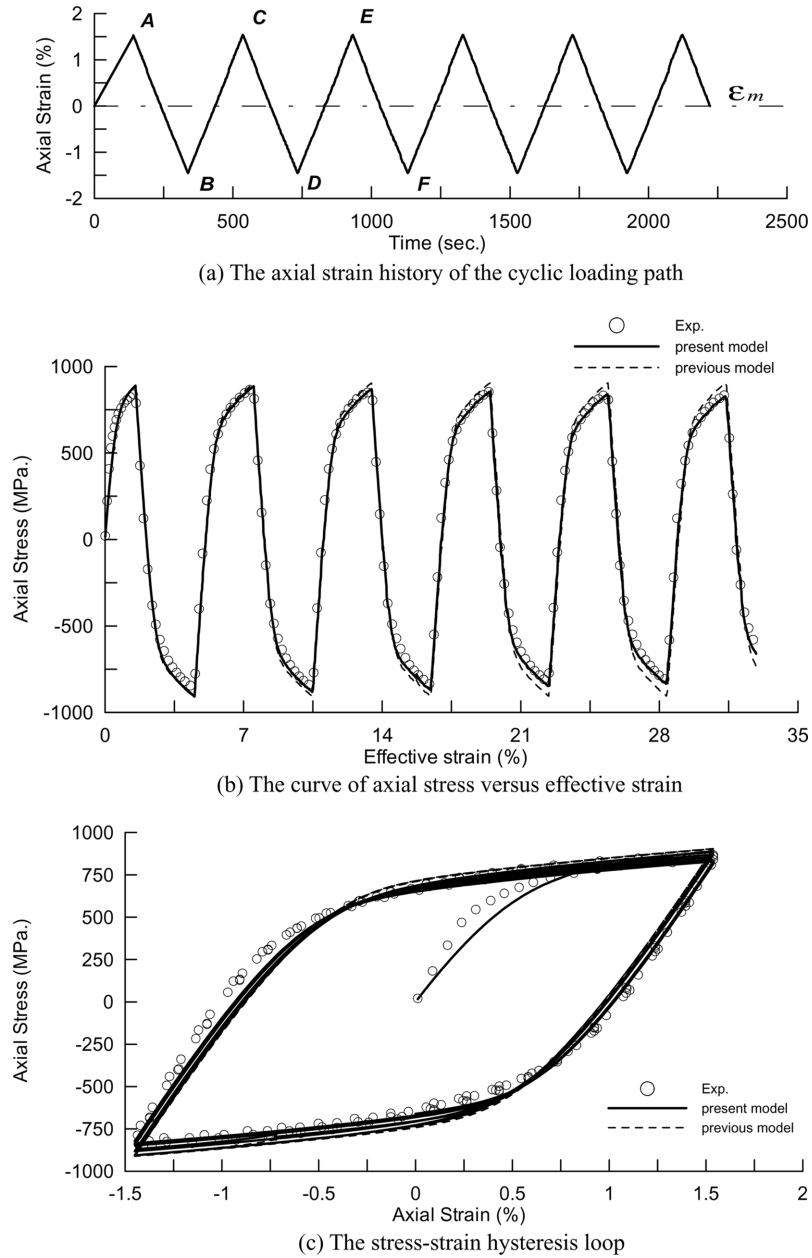


Fig. 2 SAE 4340 steel under uniaxial cyclic loading of symmetric amplitude

According to Eq. (10), the initial value of the reference intrinsic time z_{ref} is zero. Therefore, the steady value of function $c(z_{ref})$ is always equal to a constant d if materials were loaded by monotonic loading condition. In this particular consideration, the expression of Eq. (5) is recovered from Eq. (10), that is to say, the material function $f(z)$ defined by Eq. (5) is a particular form of that defined by Eq. (10). In addition, the proposed material function $f(z)$ has some characteristics depending on the choice of d and h , mentioned as follows:

- (a) As $h \geq 1$ and $d < 1$, the values of $c(z_{ref})$ and $f(z)$ versus the intrinsic time z are schematically demonstrated in Fig. 1(a) for an ideal cyclic loading path similar to that as shown in Fig. 2(a). Specifically, the saturation value $c(z_{ref})$ of material function keeps increasing in proportion to the loading cycles while the material function $f(z)$ is a decreasing function. Similarly, as $h \geq 1$ and $d > 1$, Fig. 1(b) shows that the saturation value $c(z_{ref})$ of material function keeps decreasing in proportion to the loading cycles while the material function $f(z)$ is an increasing function. It is noted that in Figs. 1(a) and (b), the sequential small letters, such as a , b , and c , correspond to the strain states, denoted by the corresponding capital letters A , B , and C , respectively as indicated in Fig. 2(a), where the cyclic loading path changes its direction.
- (b) As $0 < h < 1$ and $d < 1$, Fig. 1(c) shows that the saturation value $c(z_{ref})$ of the material function keeps increasing in proportion to the loading cycles while the material function $f(z)$ is initially a decreasing function, and then transforms into an increasing function. As $0 < h < 1$ and $d > 1$, Fig. 1(d) shows that the saturation value $c(z_{ref})$ of the material function keeps decreasing in proportion to the loading cycles while the material function $f(z)$ is initially an increasing function, and then transforms into a decreasing function. It is also noted that the small letters as shown in Figs. 1(c) and (d) correspond to the strain states as indicated by the capital letters in Fig. 2(a).
- (c) As $h < 0$ and $d < 1$, Fig. 1(e) shows that the saturation value $c(z_{ref})$ of the material function keeps decreasing in proportion to the loading cycles while $f(z)$ is always a decreasing function. As $h < 0$, and $d > 1$, Fig. 1(f) shows that the saturation value $c(z_{ref})$ of the material function keeps increasing in proportion to the loading cycles while $f(z)$ is always an increasing function.

As shown in Fig. 1, it is apparent that the initial value of $f(z)$ upon each of the reversal loadings occurring is always reset to be unity regardless of the corresponding saturation value $c(z_{ref})$, and that the property of $f(z)$ strongly depends on the choice of the combination of the material constants d and h . Accordingly, it becomes clear to us that the present model of material function as given by Eq. (10) not only behaves distinctively during each step of cyclic loading path but also is much different from any of those as shown in Eqs. (4)-(6). As previously mentioned, the material function as shown in Eq. (4) is always monotonically increasing whereas the other as shown in Eq. (5) is always either monotonically increasing if $c > 1$ or monotonically decreasing if $c < 1$. However, the function as shown in Eq. (6) is capable of being reset upon each of reversal loadings occurring, but it is merely a particular case of Eq. (10) and thus excludes all the cases as demonstrated in Fig. 1. Eq. (6) can be recovered from Eq. (10), where $c(z_{ref})$ is chosen to be a constant. In this case, the material function changes its value from 1 to the constant characterized by c during each step of the cyclic loading path.

3. Application to the combined axial-torsional case

To derive the constitutive equation for the combined axial-torsional case, the intrinsic time as shown in Eq. (1) is considered being defined in terms of plastic strain, that is, $\kappa_1 = 1$ is used in Eq. (2). Assuming that the strain components orthogonal to the axial loading direction are equal as a result of Poisson's effect, that is, $d\varepsilon_{22} = d\varepsilon_{33}$, the deviatoric stress tensor, ds_{ij} , and plastic strain tensor, $d\varepsilon_{ij}^p$, can be expressed as follows, respectively:

$$ds_{ij} = \begin{pmatrix} \frac{2}{3}d\sigma_{11} & d\sigma_{12} & 0 \\ d\sigma_{12} & -\frac{1}{3}d\sigma_{11} & 0 \\ 0 & 0 & -\frac{1}{3}d\sigma_{11} \end{pmatrix}$$

$$d\varepsilon_{ij}^p = \begin{pmatrix} \frac{2}{3}\left(d\varepsilon_{11} - d\varepsilon_{22} - \frac{d\sigma_{11}}{2\mu_0}\right) & d\varepsilon_{12} - \frac{d\sigma_{12}}{2\mu_0} & 0 \\ d\varepsilon_{12} - \frac{d\sigma_{12}}{2\mu_0} & -\frac{1}{3}\left(d\varepsilon_{11} - d\varepsilon_{22} - \frac{d\sigma_{11}}{2\mu_0}\right) & 0 \\ 0 & 0 & -\frac{1}{3}\left(d\varepsilon_{11} - d\varepsilon_{22} - \frac{d\sigma_{11}}{2\mu_0}\right) \end{pmatrix} \quad (11)$$

For realistic application, both $U(z)$ and $V(z)$ of the kernel function given by Eq. (8) only takes two terms. Therefore, they are expressed as

$$U(z) = \sum_{r=1}^2 C_r e^{-\alpha_r z} = C_1 e^{-\alpha_1 z} + C_2 e^{-\alpha_2 z}$$

$$V(z) = \sum_{r=1}^2 C_r^* e^{-\alpha_r^* z} = C_1^* e^{-\alpha_1^* z} + C_2^* e^{-\alpha_2^* z} \quad (12)$$

From Eqs. (9), one can obtain the followings for the axial-torsional case:

$$d\sigma_{11} = p_1 d\varepsilon_{11} + p_2 (d\varepsilon_{11} + 2d\varepsilon_{22}) + p_3 \left(\frac{2}{3}\right) \sum_{r=1}^2 \alpha_r (\sigma_{11})_r dz \quad (13)$$

$$d\sigma_{22} = p_1 d\varepsilon_{22} + p_2 (d\varepsilon_{11} + 2d\varepsilon_{22}) + p_3 \left(\frac{-1}{3}\right) \sum_{r=1}^2 \alpha_r (\sigma_{11})_r dz \quad (14)$$

$$d\sigma_{12} = p_1^* d\varepsilon_{12} + p_3^* \sum_{r=1}^2 \alpha_r^* (\sigma_{12})_r dz \quad (15)$$

where the summation terms on r can further be expanded step by step as follows:

$$(\sigma_{11})_r^{(k)} = \frac{3}{2} \left[(S_{11})_r + \frac{2C_r}{1 + \frac{U(0)}{u_0}} \left[\frac{2}{3} (d\varepsilon_{11} - d\varepsilon_{22}) \right] - \frac{\alpha_r (S_{11})_r}{1 + \frac{U(0)}{u_0}} dz \right]^{(k-1)}, \quad k \geq 1, r = 1, 2$$

$$(\sigma_{12})_r^{(k)} = \left[(S_{12})_r + \frac{2C_r^*}{1 + \frac{V(0)}{u_0}} d\varepsilon_{12} - \frac{\alpha_r^* (S_{12})_r}{1 + \frac{V(0)}{u_0}} dz \right]^{(k-1)}, \quad k \geq 1, r = 1, 2$$

where the stress increment $d\sigma_{22}$ always equals to zero. In step-by-step computations, the initial values of $(S_{11})_r^{(0)}$ and $(S_{12})_r^{(0)}$ were taken equal to zero since these two components correspond to free state. It is seen from Eqs. (13)-(15) that there are four unknowns, $d\sigma_{11}$, $d\sigma_{12}$, $d\varepsilon_{22}$ and dz , along with only three independent equations. Therefore, in order to solve these unknowns, an additional independent equation that will be derived subsequently is asked for.

Consider that the material is initially isotropic and obeys von Mises criterion, the material tensor K_{ijkl} for the axial-torsional case can be expressed as (Valanis 1980):

$$K_{ijkl} = \begin{pmatrix} 1 & 0 & 0 & 0 \\ 0 & 1 & 0 & 0 \\ 0 & 0 & 1 & 0 \\ 0 & 0 & 0 & 2 \end{pmatrix}$$

Direct substitution of the above equation into Eq. (1) together with the result shown in Eq. (3) lead to the additional equation:

$$d\zeta^2 = (de_{11}^p)^2 + (de_{22}^p)^2 + (de_{33}^p)^2 + 2(de_{12}^p)^2 = (f(z)dz)^2 \tag{16}$$

To determine $d\sigma_{11}$, $d\sigma_{12}$, $d\varepsilon_{22}$ and dz from the system of Eqs. (13)-(16), a numerical scheme was used. By guessing the values for the plastic strain increments de_{11}^p and de_{12}^p , denoted by $d\hat{e}_{11}^p$ and $d\hat{e}_{12}^p$, respectively, the corresponding value of $d\hat{\zeta}$ as well as $d\hat{z}$ was determined using Eq. (16). Upon determination of $d\hat{z}$, the remaining unknowns $d\hat{\sigma}_{11}$, $d\hat{\sigma}_{12}$, and $d\hat{\varepsilon}_{22}$ were simultaneously solved from the system of Eqs. (13)-(15). Finally, the plastic strain increments, $d\tilde{e}_{11}^p$ and $d\tilde{e}_{12}^p$ were calculated according to Eq. (11), where $d\sigma_{11}$, $d\sigma_{12}$, and $d\varepsilon_{22}$ were replaced by $d\hat{\sigma}_{11}$, $d\hat{\sigma}_{12}$, and $d\hat{\varepsilon}_{22}$, respectively, and then used to calculate $d\tilde{\zeta}$ using Eq. (11) again. To decide whether or not the solution of these unknowns were accepted, the criterion defined by $|d\tilde{\zeta} - d\hat{\zeta}|/d\hat{\zeta} \leq \delta$, where $|a|$ represents the absolute value of a , and δ a predetermined small value, is proposed. When the criterion had been satisfied, the solved unknowns, $d\sigma_{11}$, $d\sigma_{12}$, $d\varepsilon_{22}$ and dz were accepted; computation for current step was stopped and then went to the next step. Otherwise, the computation for the current step was iterated until the criterion would be satisfied. At the beginning of any iterative computation, the value of de_{11}^p as given by Eq. (16) was re-guessed automatically by taking the average value of $d\hat{e}_{11}^p$ and $d\tilde{e}_{11}^p$ previously determined, and so was the value of de_{12}^p . In this work, the predetermined value selected is 5%.

Table 1 Material constants and parameters of SAE4340 steel

Material constants					
μ_0 (MPa.)	K (MPa.)	C_1 (MPa.)	C_2 (MPa.)	α_1	α_2
76000	185777	168000	18500	780	100
Material parameters					
Previous model.	Eq. (5)		Present model.	Eq. (10)	
β	c	β_1	β_2	d	h
400	1.25	400	4	1.25	1.1

Table 2 Material constants and parameters of OFHC copper

Material constants					
μ_0 (MPa.)	K (MPa.)	C_1 (MPa.)	C_2 (MPa.)	C_1^* (MPa.)	C_2^* (MPa.)
43257	112807	48000	40000	32000	21000
α_1	α_2	α_1^*	α_2^*		
1200	1200	870	870		
Material parameters					
Present model.	Eq. (10)				
β_1	β_2	d	h		
1000	8	1.2	1.1		

4. Results and discussion

In the figures to be presented, the theoretical result based on the proposed model as given by Eq. (10) is represented by the solid curve with being marked by 'present model', and the experimental data represented by discrete symbols. However, in order to magnify the benefits of the present model to the prediction of cyclic plastic behavior, the theoretical result, based on the previous model proposed by Wu and Yip (1981) as shown in Eq. (5), is also presented and represented by the dashed curve with being marked by 'previous model' for comparison and discussion. The experimental results used for comparison are due to Shiao (2000), who conducted the circular rod specimens of SAE4340 alloy steel on a servo-controller hydraulic MTS809 test machine. Five specimens were tested under strain control of uniaxial cyclic loading with various amplitudes, respectively. The determined material constants and parameters of present and previous models are listed in Table 1, respectively. In this table, only the constants corresponding to the axial behavior are required for the uniaxial case as mentioned above. In addition, the capability and validity of the present model in predicting the plastic behavior of erasure of memory of materials are verified using the experimental result of Lamba and Sidebottom (1978) in a subsequent section. In the work of Lamba and Sidebottom (1978), the specimen made of OFHC (oxygen free high conductivity) copper was tested under combined axial-torsional strain control, for which the determined constants are listed in Table 2.

4.1 Uniaxial cyclic loading of symmetric amplitude

In this case, the specimen made of SAE 4340 alloy was subjected to the uniaxial cyclic loading condition of symmetric amplitude, as shown in Fig. 2(a). The loading amplitude of the axial strain is about $\pm 1.5\%$ cyclically repeated for 5 cycles. Note that in Fig. 2(a) and also in another figures to be presented, the center line denoted by ε_m represents the history of mean strain in the cyclic loading process. Shown in Figs. 2(b) and (c) is the comparison between the theoretical and experimental results. We do show the curve of the axial stress versus the effective strain, defined by $\sqrt{2\varepsilon_{ij}\varepsilon_{ij}/3}$ where ε_{ij} is the total strain tensor, in Fig. 2(b) for the ease of comparison. It is observed from the experimental result of stress-strain hysteresis loops that the material has a little cyclic hardening before arriving at steady state phenomenon. The predictions of the cyclic hardening

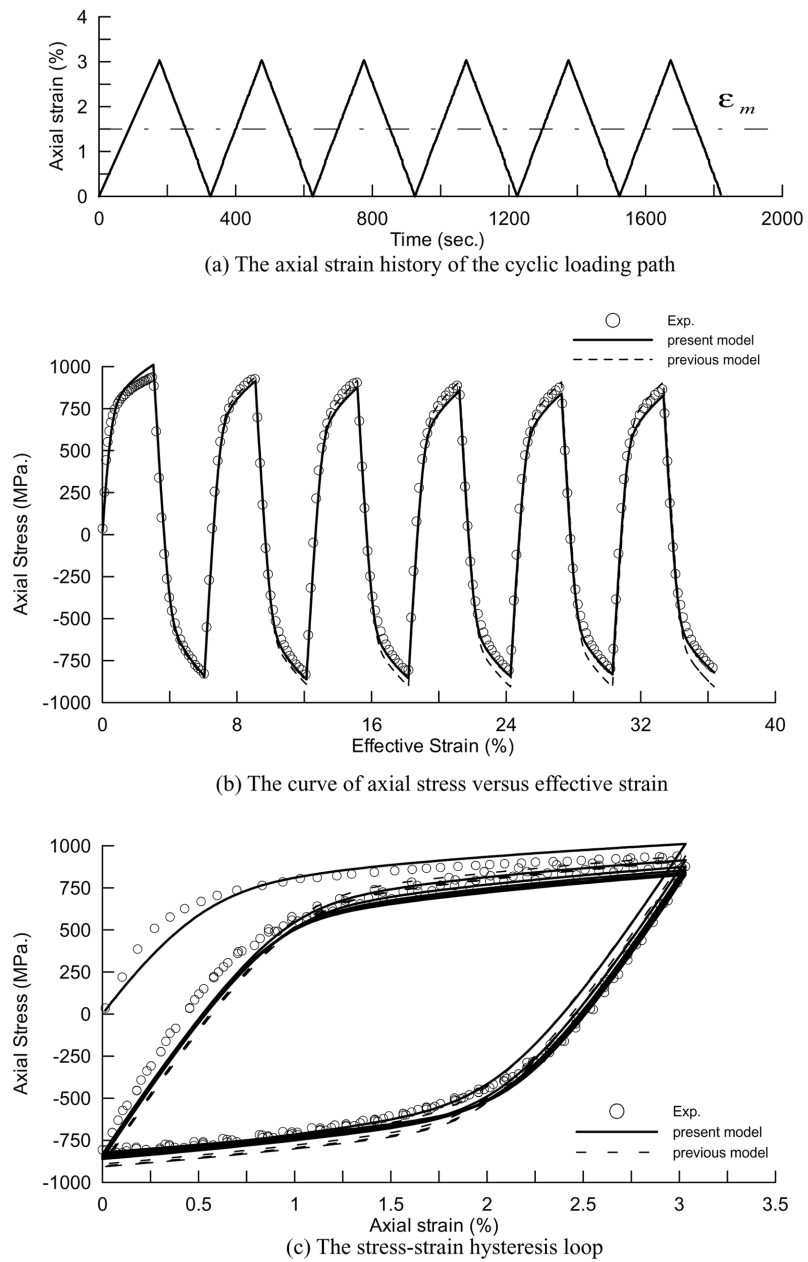


Fig. 3 SAE 4340 steel under uniaxial cyclic loading of asymmetric amplitudes

behavior according to the present and previous models are both in reasonable agreement with experimental results. However, as shown in Figs. 2(b) and (c), the theoretical result based on present model is better, especially in predicting the evolution of peak stress during plastic deformation process.

4.2 Uniaxial cyclic loading of asymmetric amplitudes

As shown in Fig. 3(a), this specimen was loaded by the uniaxial loading condition of asymmetric amplitudes, cyclically repeated between 0 and +3% for five cycles. Shown in Figs. 3(b) and (c) is the comparison between the theoretical and experimental results. From these figures, it is experimentally observed that the evolution of peak stress value gradually keeps decreasing as the cyclic loading proceeds. It is also seen that the present model describes such an observed cyclic

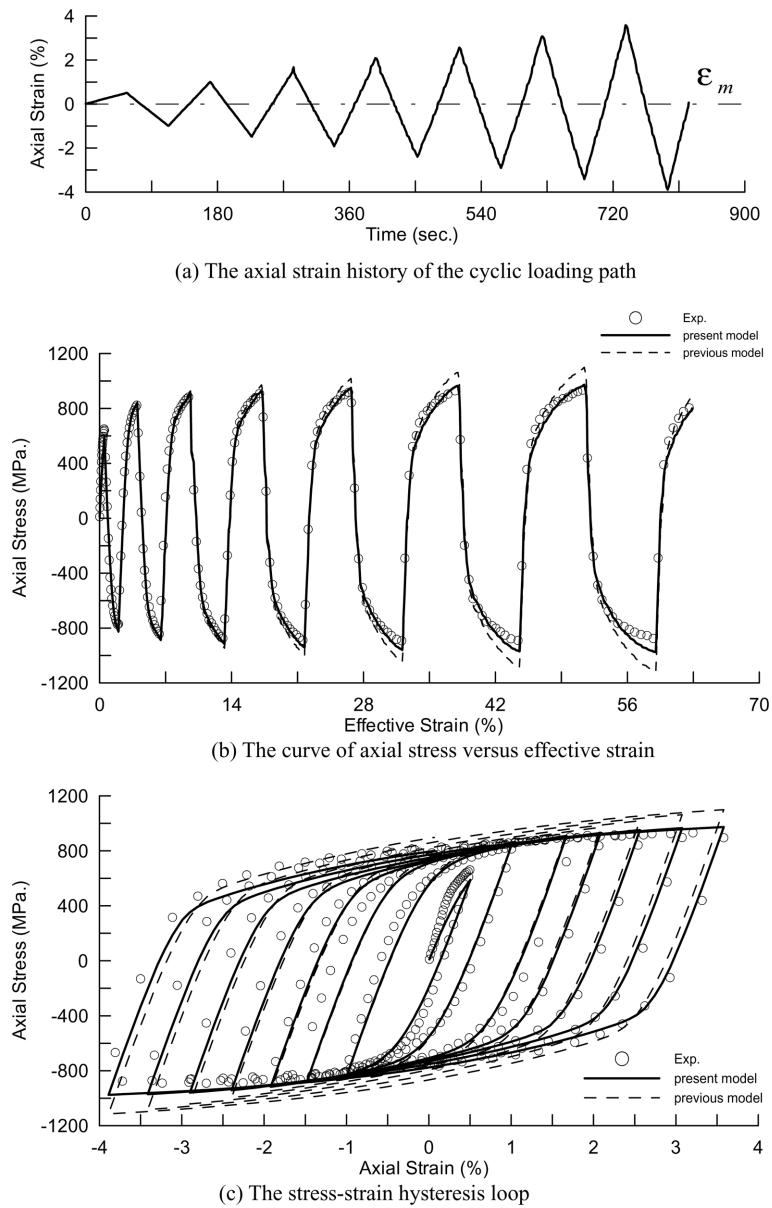


Fig. 4 SAE 4340 steel under uniaxial cyclic loading path with progressively increasing amplitudes

behavior much better than the previous one. Specifically, due to the determined parameters for d and h as listed in Table 1, the material function of the model as given by Eq. (10) clearly belongs to the category as schematically represented in Fig. 1(b). Alternatively, with the parameters chosen the present model leads to the material function $f(z)$ which complies with the experimental observation, because that in this case $f(z)$ is not only an increasing function during each step of the cyclic loading path but also characterized by the saturation value $c(z_{ref})$ gradually decreasing as the loading proceeds. On the other hand, when the previous model as given by Eq. (5) is employed, it leads to the corresponding $f(z)$ which is monotonically increasing throughout. This, however, does not qualitatively reflect the fact as experimentally found.

4.3 Uniaxial cyclic loading with progressively increasing amplitudes

As shown in Fig. 4(a), the specimen was loaded following the uniaxial cyclic loading path with progressively increasing amplitudes; the loading path increases its amplitude of the axial strain by +0.5% per half a cycle until the axial strain is accumulated to 4%. Figs. 4(b) and (c) show the comparison between the theoretical and experimental results. The experimental stress-strain hysteresis loops are found to be progressively extending along with the increasing strain amplitude. The present model obviously describes such experimental observations better than the previous one also. Specifically, by comparing the deviation existing between the theoretical and experimental results, especially in peak stress values, it is found that much more deviation is observed when the previous model is employed theoretically. In other words, the theoretical prediction is apparently improved by the present model, especially in the peak stress, experimentally observed to evolve along with increasing number of the cyclic loading. Also, it is seen from Figs. 4(b) and (c) that the present model is better than the previous one in predicting the Bauschinger effect, which reflects to the “knee” portion of the stress-strain hysteresis loops.

As mentioned before, although the present model has led to the material function $f(z)$ which keeps its saturation value, dominated by $c(z_{ref})$, decreasing during each step of the cyclic loading path as long as the cyclic loading proceeds, yet the extended stress-strain hysteresis is predicted appropriately. This is because that on one hand, with the determined parameter β_1 as listed in Table 1, the $f(z)$ value would never saturate during each step of the loading path, and on the other hand the magnitude of the peak stress value is not only path-dependent, but also dependent on the deformation history of that step loading.

4.4 Uniaxial cyclic loading with various mean amplitudes

As shown in Fig. 5(a), the specimen made of SAE4340 alloy was uniaxially loaded following the cyclic loading path with various mean amplitudes. The mean amplitude of the axial strain gradually increases from 0 to 6%, and then gradually decreases to 0; the difference of the corresponding peak values of the axial strain between contiguous cycles keeps 0.6%. Figs. 5(b) and (c) show the comparison between the theoretical and experimental results. The material under this loading condition experimentally behaves as described subsequently. During the cycles where the mean amplitude of the axial strain keeps increasing, the stress-strain hysteresis loop is observed to move up and right simultaneously. This turns out to make the magnitude of the peak stress increasing in tension and decreasing in compression. During the remaining cycles of the loading path where the mean amplitude of the strain keeps decreasing, the motion of the loop, however, looks completely

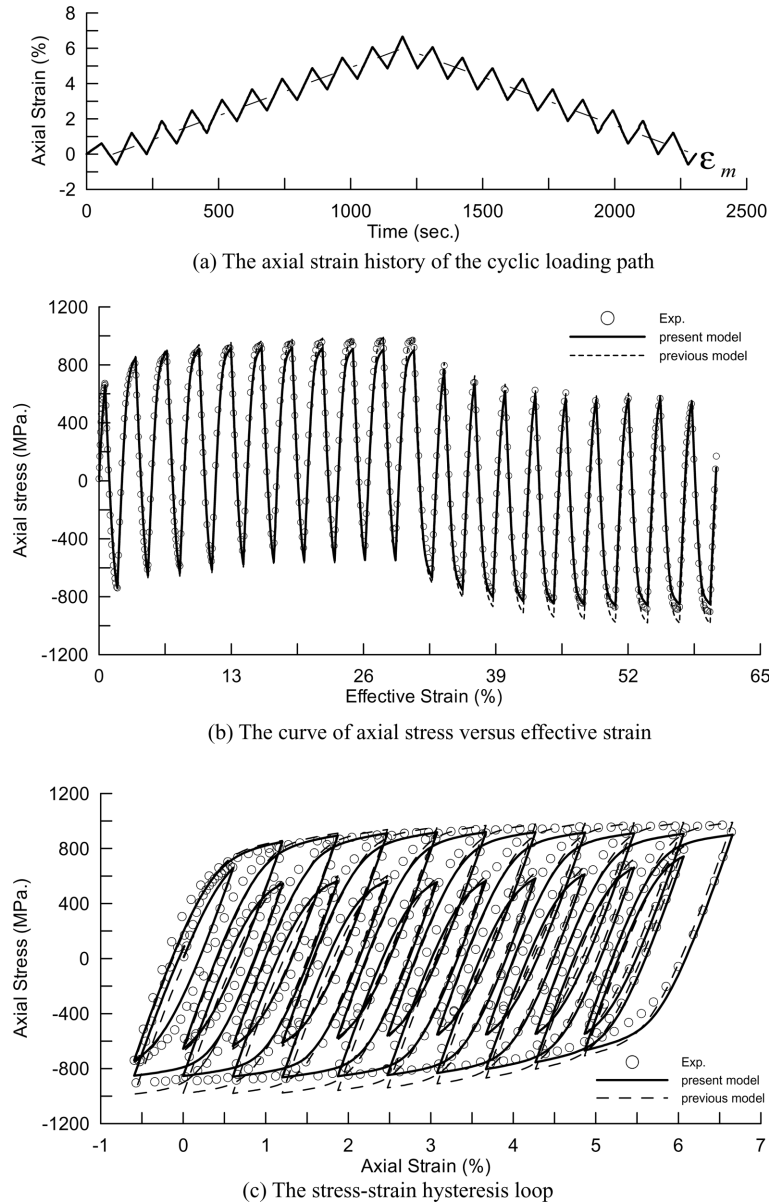


Fig. 5 SAE 4340 steel under uniaxial cyclic loading path with various mean amplitudes

opposite to that observed initially. The cyclic behavior, above described, is qualitatively described well by both of the models. However, as long as the quantitative analysis is concerned, it can be seen from these two figures that the present model predicts not only the peak stress, especially corresponding to the compression of the remaining cycles, closer to the experiment, but also the Bauschinger effect more appropriately in the cyclic loading process. It is fair to say that the theoretical prediction is significantly improved by using the present model.

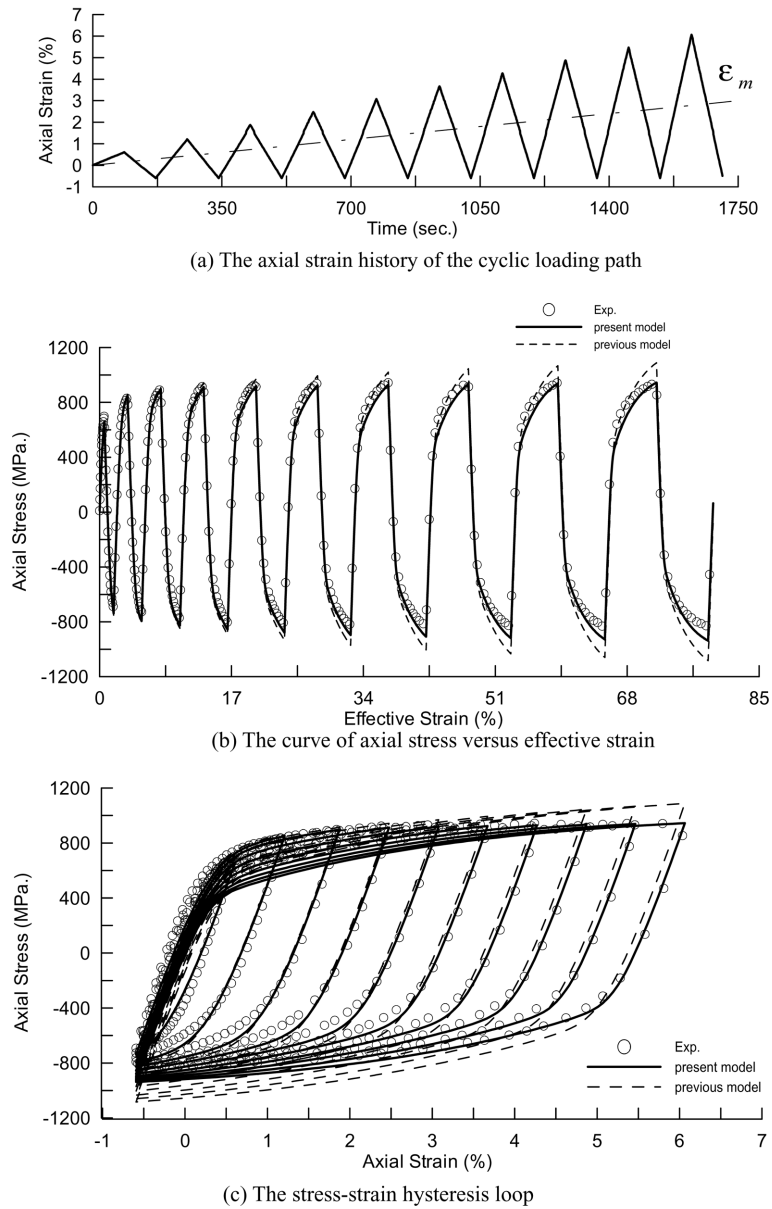
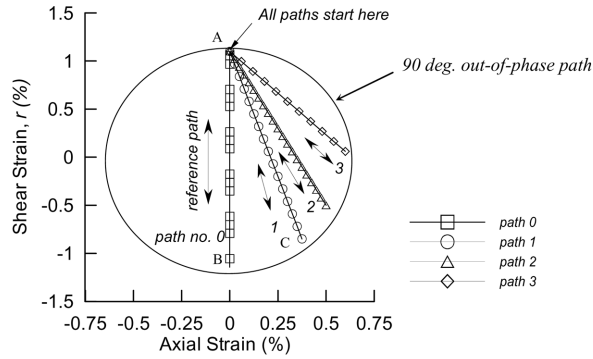


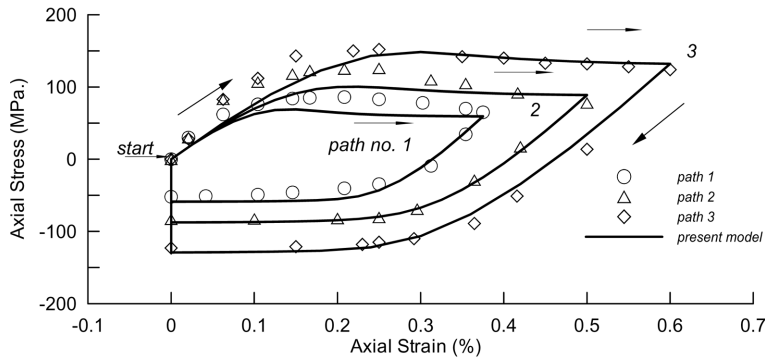
Fig. 6 SAE 4340 steel under uniaxial cyclic loading path with increasing mean amplitudes

4.5 Uniaxial cyclic loading with increasing mean amplitudes

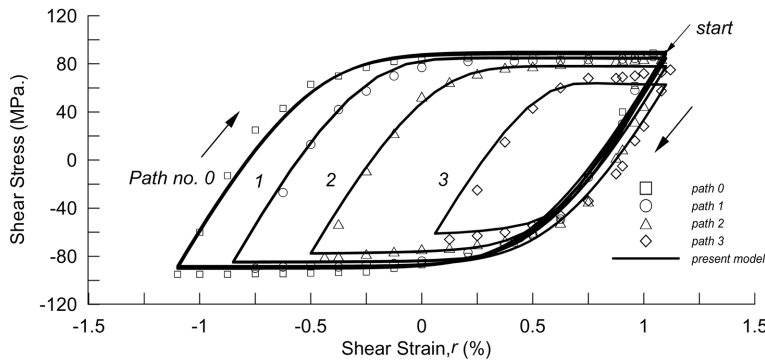
As shown in Fig. 6(a), the specimen was uniaxially loaded by the cyclic loading with increasing mean amplitudes; the amplitude of the axial strain in tension progressively increases from 0.6% to 6% at a fixed amount of 0.6% per cycle while the amplitude of the axial strain in compression remains - 0.6%. Figs. 6(b) and (c) show the comparison between the theoretical and experimental results. The experimental result is observed such that as the cyclic loading proceeds, the stress-strain



(a) Strain control program for subsequent strain hardening after torsional cycle (path sequence 0-1-0-1-0-2-0-2- etc.)



(b) Subsequent strain hardening after torsional cycle -Axial behavior



(c) Subsequent strain hardening after torsional cycle -torsional behavior

Fig. 7 Simulation of erasure of memory of OFHC copper

hysteresis loop extends gradually while shifting apparently towards the right hand side of the axial strain coordinate. Although such experimental observations are qualitatively described well by both models, yet the present model based on Eq. (10) clearly arrives at a better result both in predicting the Bauschinger effect as well as the evolution of the peak stress. The reason why the present model improves the theoretical prediction is mainly due to its behavior in similarity to what is shown in Fig. 1(b).

4.6 Erasure of memory of materials

In an effort to verify the proposed model of material function as given by Eq. (10), the experimental result of Lamba and Sidebottom (1978) from the specimen made of OFHC copper is used. The specimens, made of OFHC copper, used in Lamba and Sidebottom (1978), were annealed in vacuum at 1030°F (554°C) for one hour and then furnace cooled. Accordingly, we assume the material is initially isotropic, and thus the definition of intrinsic time measure K_{ijkl} (with 1 and 2) was employed in numerical computation to comply with the initial property of the material. The specimen was loaded under strain control following the loading path as shown in Fig. 7(a). It was first cycled torsionally (not shown in Fig. 7(a)) and then fully stabilized under 90 deg out-of-phase cycling. It was then subjected to a reverse shear strain loading called reference path 0 (A-B-A in Fig. 7(a)) for which the peak shear strain was approximately 95 percent of that at which initial cyclic hardening occurred, and finally subjected to cyclic path sequence 0-1-0-1-0-2-0-2-etc. It is noted that the specimen was loaded in such a manner that the ‘big’ path is intervened between each smaller paths, such as path 1 denoted by A-C-A and path 2 denoted by A-D-A in Fig. 7(a). Corresponding to the loading path as shown in Fig. 7(a), the theoretical prediction compared with the experimental result is based on the present model, and is shown in Figs. 7(b) and (c) for the axial and shear behavior, respectively. We note that in theoretical simulation, the computation had been accomplished according to 90 degree out-of-phase experimental cycling until the stress-strain hysteresis loops were fully stabilized before the stress responses to strain paths 0-1-0-1-0-2-0-2-etc. were computed. Since the present model is basically a macroscopic phenomenological approach, the loading history of 90 degree out-of-phase cycling may be legally accounted for in the manner, above mentioned. We note that in these two figures, only the stress-strain hysteresis loops under subsequent strain paths as denoted by 0-1-0-1-0-2-0-2-etc., after the material was fully stabilized under 90 degree out-of-phase cycling, are presented for the purpose of clarity. Clearly, it can be seen from these figures that the theoretical stress-strain hysteresis loops corresponding to the same smaller paths (e.g. path1 and next path1) are indistinguishable due to the reference path 0 preceding them each time. Specifically, the stress state is brought back to the point as indicated by ‘start’ in the figures as long as the material is reloaded completely by the reference path 0 after any of the smaller paths (path1,2,3). Theoretically, the reference path 0 is shown to apparently ‘wash’ out the influence of the preceding smaller paths, as observed experimentally. In addition, the theoretical prediction is in a satisfactory agreement with the experimental result.

Alternatively, the result shown in Fig. 7 clearly indicates that the present model is capable of predicting ‘erasure of memory of materials’ as found experimentally. This is because that the present model as given by Eq. (10) always resets the value of $f(z)$ to be unity whenever the loading path changes its direction, and also that the saturation value of $c(z_{ref})$ becomes a nearly constant after the material has arrived at steady state, characterizing that the reference time z_{ref} at any moment after the steady state is sufficiently large. Accordingly, corresponding to the same smaller paths between which the reference path 0 intervenes, the relation of $f(z)$ versus the intrinsic time defined by $(z - z_{ref})$ almost keeps unchanged, also making the computed stress trajectories almost identical for the same path. We note that from Eq. (10), the function $c(z_{ref})$ approaches to a constant defined by $(h - 1)d + 1/h$ when z_{ref} is large enough. However, the previous model is unable to predict ‘the erasure of memory of materials’ since the function given by Eq. (5) can never reset upon the loading path abruptly changing its direction. Due to this reason, the theoretical prediction based on the previous model is omitted.

5. Conclusions

In this article, associated with the endochronic theory of plasticity of the differential form, the material function as given by Eq. (10) is proposed, and applied to predict the cyclic plastic behavior of SAE 4340 steel, uniaxially loaded both symmetrically and asymmetrically with various amplitudes. In addition to compare with the experimental result obtained by Shiao (2000), the theoretical prediction employing the present model is also compared with the one using the previous model as shown in Eq. (5). Through the comparison and discussions, it is fair to conclude that the present model considerably improves on the previous one, especially in the prediction of the Bauschinger effect as well as the peak stress evolved along with the cyclic loading path proceeding. In addition, the present model has successfully shown to be capable of describing the so-called ‘erasure of memory of materials’, as experimentally observed by Lamba and Sidebottom (1978).

The main distinction between the present (Eq. (10)) and previous (Eq. (5)) models is that rather than a constant as Eq. (5) demands, the present model expresses the parameter $c(z_{ref})$ as a function of the reference intrinsic time z_{ref} , corresponding to which the loading direction changes. Therefore, the present model can substantially result in six categories of the material function depending on the choice of the combination of the constants d and h , each of which can behave differently with respect to an identical deformation history, as schematically shown in Fig. 1. In particular, the previous models as given by Eqs. (5) and (6) can both be recovered from the present one. Furthermore, according to the determined constants d and h as listed in Table 1, the cyclic plastic behavior of SAE 4340 steel belongs to the category as shown in Fig. 1(b). Therefore, in order to broaden the capability and validity of the present model, further work for additional verification of the model is required by pursuing the cyclic plastic behavior of materials belonging to another category as described in Fig. 1.

References

- Basuroychowdhury, I.N. and Voyiadjis, G.Z. (1998), “A multiaxial cyclic plasticity model for nonproportional loading cases”, *Int. J. Plasticity*, **14**, 855-870.
- Beaudoin, A.J., Dawson, P.R., Mathur, K.K., Kocks, U.F. and Korzekwa, D.A. (1991), “Application of polycrystalline plasticity to sheet forming”, *Comp. Math. Appl. Mech. Eng.*, **117**, 49-70.
- Cailletaud, G. (1984), “Some elements on multiaxial behavior of 316L stainless steel at room temperature”, *Mech. Mater.*, **3**, 333-345.
- Calloch, S. and Marquis, D. (1997), “Additional hardening due to tension-torsion nonproportional loadings: influence of the loading shape; multiaxial fatigue and deformation testing techniques”, In: Kalluri, S., Bonacuse, P.J.(Eds.) ASTM STP 1280. American Society for Testing and Materials, 113-130.
- Chang, K.C. and Lee, G.C. (1986), “Biaxial properties of structural steel under nonproportional loading”, *J. Eng. Mech.*, **112**, 792-805.
- Dafalias, Y.F. and Aifantis, E.C. (1990), “On the microscopic origin of the plastic spin”, *Acta Mech.*, **82**, 31-48.
- Dafalias, Y.F. and Popov, E.P. (1976), “Plastic internal variables formalism of plasticity”, *J. Appl. Mech.*, **43**, 645-651.
- Diard, O., Leclercq, S., Rousselier, G. and Cailletaud, G. (2005), “Evaluation of finite element based analysis of 3D multicrystalline aggregates plasticity: Application to crystal plasticity model identification and the study of stress and strain fields near grain boundaries”, *Int. J. Plasticity*, **21**, 691-722.
- Ellyin, F. and Wolodko, J.D. (1997), “Testing facilities for multiaxial loading of tubular specimens, multiaxial

- fatigue and deformation testing techniques”, ASTM STP 1280, S. Kalluri and P.J. Bonacuse, Eds., ASTM, 7-24.
- Hopperstad, O.S., Langseth, M. and Remseth, S. (1995a), “Cyclic stress-strain behaviour of alloy AA6060 T4, Part I: Biaxial experiments and modeling”, *Int. J. Plasticity*, **11**, 725-739.
- Hopperstad, O.S., Langseth, M. and Remseth, S. (1995b), “Cyclic stress-strain behaviour of alloy AA6060 T4, Part II: Biaxial experiments and modeling”, *Int. J. Plasticity*, **11**, 741-762.
- Krempf, E. and Lu, H. (1984), “The hardening and rate dependent behavior of fully annealed AISI type 304 stainless steel under biaxial in-phase and out-of-phase strain cycling at room temperature”, *J. Eng. Mater. Technol.*, **106**, 376-384.
- Krieg, R.D. (1975), “A practical two surface plasticity theory”, *J. Appl. Mech.*, **42**, 641-646.
- Kwofie, S. (2003), “Description of cyclic hysteresis behavior based on one-parameter model”, *Mater. Sci. Eng.*, **A357**, 86-93.
- Lamba, H.S. and Siderbottom, O.M. (1978), “Cyclic plasticity for nonproportional path: Part 1: Cyclic hardening, erasure of memory, and subsequent strain hardening experiments”, *J. Eng. Mater. Technol.*, **100**, 96-103.
- Miehe, C., Schotte, J. and Schroder, J. (1999), “Computational micro-macro transitions and overall moduli in the analysis of polycrystals at large strains”, *Comput. Mat. Sci.*, **16**, 372-382.
- Mroz, Z. (1967), “On the description of anisotropic workhardening”, *J. Mech. Phys. Solids*, **15**, 163-175.
- Murakami, H. and Read, H.E. (1989), “A second-order numerical scheme for integrating the endochronic plasticity equations”, *Comput. Struct.*, **31**, 663-672.
- Ning, J. and Aifantis, E.C. (1996), “Anisotropic yield and plastic flow of polycrystalline solids”, *Int. J. Plasticity*, **12**, 1221-1240.
- Pan, W.F. and Chern, C.H. (1997), “Endochronic description for viscoplastic behavior of materials under multiaxial loading”, *Int. J. Solids Struct.*, **34**, 2131-2160.
- Pan, W.F. and Chiang, W.J. (1999), “Endochronic analysis for rate-dependent elasto-plastic deformation”, *Int. J. Solids Struct.*, **36**, 3215-3237.
- Rivlin, R.S. (1981), “Some comments on the endochronic theory of plasticity”, *Int. J. Solids Struct.*, **17**, 231-248.
- Samson, Y., Hong S.G. and Lee, S.B. (2004), “Phenomenological description of cyclic deformation using the overlay model”, *Mater. Sci. Eng.*, **A364**, 17-26.
- Sandler, I.S. (1978), “On the uniqueness and stability of endochronic theories of material behavior”, *J. Appl. Mech.*, **45**, 263-266.
- Shiao, Y.P. (2000), “A study on multiaxial cyclic loading and anisotropic plasticity of structural metals”, Ph.D. Thesis, National Taiwan University, Dept. of C.E.
- Tanaka, E., Murakami, S. and Ooka, M. (1985a), “Effects of strain path shapes on non-proportional cyclic plasticity”, *J. Mech. Phys. Solids*, **33**(6), 559-575.
- Tanaka, E., Murakami, S. and Ooka, M. (1985b), “Effects of plastic strain amplitudes on non-proportional cyclic plasticity”, *Acta Mech.*, **57**, 167-192.
- Valanis, K.C. (1971), “A theory of viscoplasticity without a yield surface, Part I: General theory”, *Arch. Mech.*, **23**, 517-551.
- Valanis, K.C. (1980), “Fundamental consequence of a new intrinsic time measure-plasticity as a limit of the endochronic theory”, *Arch. Mech.*, **32**, 171-191.
- Valanis, K.C. and Fan, J. (1983), “Endochronic analysis of cyclic elastoplastic strain fields in a notch plate”, *J. Appl. Mech.*, ASME, **50**, 789-794.
- Valanis, K.C. (1984), “Continuum foundations of endochronic plasticity”, *J. Eng. Mater. Technol.*, **106**, 367-375.
- Watanabe, O. and Atluri, S.N. (1986), “Constitutive modeling of cyclic plasticity and creep, using an internal time concept”, *Int. J. Plasticity*, **2**, 107-134.
- Wu, H.C., Yao, J.C. and Chu, S.C. (1986), “Investigation of endochronic constitutive equation subject to plastic strain-controlled axial-torsional deformation”, *J. Eng. Mater. Technol.*, **108**, 262-269.
- Wu, H.C. and Yip, M.C. (1981), “Endochronic description of cyclic hardening behavior of metallic material”, *J. Eng. Mater. Technol.*, **103**, 212-217.
- Yeh, W.C. (1995), “Verification of the endochronic theory of plasticity under biaxial load”, *J. the Chinese Institute of Engineers*, **18**(1), 25-34.
- Yeh, W.C., Cheng J.Y. and Her, R.S. (1994), “Analysis of plastic behavior to cyclically uniaxial tests using an

- endochronic approach”, *J. Eng. Mater. Technol.*, ASME, **116**, 62-67.
- Yeh, W.C., Ho, C.D. and Pan, W.F. (1996), “An endochronic theory accounting for deformation induced anisotropy”, *Int. J. Plasticity*, **12**, 987-1004.